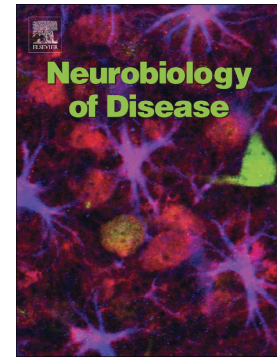


Lateral habenula dysfunctions in Tm4sf2<sup>-/-</sup> mice model for neurodevelopmental disorder

Murru Luca, Ponzoni Luisa, Longatti Anna, Mazzoleni Sara, Giansante Giorgia, Bassani Silvia, Sala Mariaelvina, Passafaro Maria



PII: S0969-9961(20)30464-2

DOI: <https://doi.org/10.1016/j.nbd.2020.105189>

Reference: YNBDI 105189

To appear in: *Neurobiology of Disease*

Received date: 10 September 2020

Revised date: 30 October 2020

Accepted date: 17 November 2020

Please cite this article as: M. Luca, P. Luisa, L. Anna, et al., Lateral habenula dysfunctions in Tm4sf2<sup>-/-</sup> mice model for neurodevelopmental disorder, *Neurobiology of Disease* (2020), <https://doi.org/10.1016/j.nbd.2020.105189>

This is a PDF file of an article that has undergone enhancements after acceptance, such as the addition of a cover page and metadata, and formatting for readability, but it is not yet the definitive version of record. This version will undergo additional copyediting, typesetting and review before it is published in its final form, but we are providing this version to give early visibility of the article. Please note that, during the production process, errors may be discovered which could affect the content, and all legal disclaimers that apply to the journal pertain.

## Lateral habenula dysfunctions in *Tm4sf2*<sup>-/-</sup> mice model for neurodevelopmental disorder

Murru Luca<sup>a,b,\*</sup> luca.murru@in.cnr.it, Ponzoni Luisa<sup>c,#1</sup>, Longatti Anna<sup>a,1</sup>, Mazzoleni Sara<sup>a,c</sup>, Giansante Giorgia<sup>a</sup>, Bassani Silvia<sup>a,b</sup>, Sala Mariaelvina<sup>a,b</sup>, and Passafaro Maria<sup>a,b,\*</sup> maria.passafaro@in.cnr.it

<sup>a</sup>Institute of Neuroscience, CNR, Milan 20129, Italy.

<sup>b</sup>NeuroMI Milan Center for Neuroscience, Università Milano-Bicocca, Milan 20126, Italy

<sup>c</sup>Department of Medical Biotechnology and Translational Medicine, Università di Milano, Segrate (MI) 20090, Italy.

\*Corresponding authors at: Institute of Neuroscience, CNR, Milan 20129, Italy.

### Abstract

Mutations in the *TM4SF2* gene, which encodes TSPAN7, cause a severe form of intellectual disability (ID) often comorbid with autism spectrum disorder (ASD). Recently, we found that *TM4SF2* loss in mice affects cognition. Here, we report that *Tm4sf2*<sup>-/-</sup> mice, beyond an ID-like phenotype, display altered sociability, increased repetitive behaviors, anhedonic- and depressive-like states. Cognition relies on the integration of information from several brain areas. In this context, the lateral habenula (LHb) is strategically positioned to coordinate the brain regions involved in higher cognitive functions. Furthermore, in *Tm4sf2*<sup>-/-</sup> mice we found that LHb neurons present hypoexcitability, aberrant neuronal firing pattern and altered sodium and potassium voltage-gated ion channels function. Interestingly, we also found a reduced expression of voltage-gated sodium channel and a hyperactivity of the PKC-ERK pathway, a well-known modulator of ion channels activity, which might explain the functional phenotype showed by *Tm4sf2*<sup>-/-</sup> mice LHb neurons.

These findings support *Tm4sf2*<sup>-/-</sup> mice as useful in modeling some ASD-like symptoms. Additionally, we can speculate that LHb functional alteration in *Tm4sf2*<sup>-/-</sup> mice might play a role in the disease pathophysiology.

---

<sup>1</sup> #These authors contribute equally to the work

**Keywords:** Lateral habenula, TSPAN7, Intellectual disability, autism spectrum disorder, neurodevelopmental disorders.

## 1. Introduction

Mutations in many genes have been linked to increased risk of developing ID and ASD so far (Mefford et al., 2012; Aspromonte et al., 2019), including the X-linked gene *TM4SF2* which encodes for tetraspanin7 (TSPAN7) protein (Piton et al., 2011; Bassani et al., 2013; Penzes et al., 2013). Patients displaying mutated *TM4SF2* gene are occasionally diagnosed for both pathologies (Piton et al., 2011), consistently with the existing comorbidity between ID and ASD (Oeseburg et al., 2011; Schwartz and Neri, 2012).

TSPAN7 is widely expressed in the central nervous system (CNS) (Zemni et al., 2000) and belongs to the tetraspanins family of proteins. Tetraspanins are transmembrane proteins structurally composed by four transmembrane domains (TM), a small and a large extracellular loop (SEL and LEL, respectively), and intracellular N- and C-termini (Berditchevski, 2001). Beyond the role in immune system, cancer progression and metastatic processes, recently tetraspanins gained much attention as synaptic regulators (Murru et al., 2018). Indeed, these proteins act as molecular facilitators interacting with other proteins, such as cell adhesion and signalling molecules (Bassani and Ciriojani, 2012; Termini and Gillette, 2017; Moretto et al., 2019), membrane receptors (Lee et al., 2017; Murru et al., 2017), ion channels (Mallmann et al., 2013), and with each other (Charrin et al., 2014), forming the Tetraspanin Enriched Microdomains (TEMs). In this way, tetraspanins favor the clusterization of membrane protein and their chance of interactions.

Previously, we demonstrated that TSPAN7 is important for synapse formation and function, identifying protein interacting with C kinase 1 (PICK1) as a direct interactor of TSPAN7 (Bassani et al., 2012). Recently, using a knockout mouse model for *Tm4sf2* (*Tm4sf2<sup>-/-</sup>*), we found that TSPAN7 plays a key role in hippocampal excitatory synapse formation, function and plasticity as well as in learning and memory (Murru et al., 2017).

In the last years, the lateral habenula (LHb) has emerged as an epithalamic region strategically positioned to integrate the information coming from different brain areas involved in a wide range of motivational, motor and higher order cognitive functions (Ji and Shepard, 2007; Goutagny et al., 2013; Namboodiri et al., 2016; Benekareddy et al., 2018). In accordance, LHb has been reported to be involved in behavioral flexibility (Baker and

Mizumori, 2017; Mizumori and Baker, 2017), sociability (Benekareddy et al., 2018), learning and memory (Lecourtier et al., 2004; Bromberg-Martin et al., 2010; Shumake et al., 2010) that are often impaired in ID and ASD patients (Moretto et al., 2018). Here, we report that  $Tm4sf2^{-/-}$  mice, beyond an ID-like phenotype (Murru et al., 2017a), display altered sociability, increased repetitive behaviors, anhedonic- and depressive-like states. Furthermore, we found that LHb neurons of  $Tm4sf2^{-/-}$  mice show reduced excitability, aberrant neuronal firing pattern and altered sodium and potassium voltage-gated ion channels function. Interestingly, we also found a reduced expression of voltage-gated sodium channel and a hyperactivity of the PKC-ERK pathway, a well-known modulator of ion channels activity, which might contribute to the functional phenotype showed by  $Tm4sf2^{-/-}$  mice LHb neurons. These findings indicate that  $Tm4sf2^{-/-}$  mice phenocopy the behavioral alterations displayed by patients carrying  $tm4sf2$  mutation, making it suitable to model the human pathology.

## 2. Materials and Methods

### 2.1. Animals

C57Bl/6  $Tm4sf2^{+/y}$  and  $Tm4sf2^{-/-}$  male mice were housed in polycarbonate cages with food and water *ad libitum*. Cob-bedding was changed weekly, and mice were maintained under a 12h light cycle (lights on at 08:00) at 21 °C. All the experiments followed the guidelines established by the Italian Council on Animal Care and were approved by the Italian Government decree No. 747/2015-PR. All efforts were made to minimize the number of subjects used and their suffering. 6-12 mice per genotype were used for behavioral testing, 5-14 for electrophysiology and 2-9 mice per genotype for biochemical analysis.

### 2.2. Behavioral tests

All behavioral tests were performed on 60-90 days old male mice. The experiments were carried out during the light phase of the cycle. All the tasks were videotaped and then the parameters for the different tests were scored.

#### 2.2.1. Repetitive self-grooming

Each mouse was individually placed into a standard empty cylinder (46 cm length × 23.5 cm wide × 20 cm high) and repetitive self-grooming behavior was assessed as previously described (McFarlane et al., 2008). The tests were performed in a ~40 lux illuminated room and the sessions were recorded with a front-mounted closed-circuit TV camera (Security Cameras Direct) placed at ~1 m from the cage. Sessions were videotaped for 20 min and the

total time spent grooming during the last 10 min and the total number of grooming episodes were measured.

### **2.2.2. Marble-burying test.**

The marble-burying test is widely used to investigate repetitive behavior in mouse, taking advantage of the rodents inclination in digging (Amodeo et al., 2012; Silverman et al., 2015). After 1 h for room acclimation, each mouse was placed in a cage (26 × 20 × 14 cm) and subjected to 30 min of habituation. Afterwards, the mouse was removed and 20 marbles equally distributed were placed on top of the bedding (5 cm in depth). Finally, each mouse was placed again in the cage for 15 min and the buried marbles were counted, measuring also the latency to the first marble burial.

### **2.2.3. Tube dominance test.**

The Tube Dominance test assesses social dominance through the measurement of aggression. Tm4sf2<sup>+/y</sup> and Tm4sf2<sup>-/y</sup> mice were released into opposite ends of a clear, narrow tube, where they can freely interact. The mouse showing greater aggression will force its opponent out of the tube. Only when one mouse has all four paws out of the tube the match ended, and the animal remaining inside the tube is declared the winner. The aggressive behavior was scored as a percentage of wins on the total number of matches.

### **2.2.4. Three-chamber sociability test.**

The test apparatus was a rectangular, three-chambered transparent polycarbonate box (width = 42.5 cm; height = 22.2 cm; center chamber, length = 17.8; side chambers, length = 19.1 cm). The tested mouse was firstly placed in the center chamber allowing the exploration of the apparatus for 10 minutes (habituation). Afterwards, a stranger mouse was placed inside a cage in the left compartment while an empty cage (the object) was placed in the right one. The time spent interacting (sniffing) with the stranger mouse or the object was monitored for 10 min.

### **2.2.5. Sucrose preference test.**

In order to investigate the ability of mice to experience pleasure, their relative preference for sucrose over water was assessed using the two-bottle choice procedure. In this test, Tm4sf2<sup>+/y</sup> and Tm4sf2<sup>-/y</sup> mice were singly housed for six days. During the first two days, the animals had free access to one bottle containing water and the 24h fluid intake was monitored. The next two days were used for habituating mice to the concomitant presence of two bottles (filled with water) and the total fluid intake was also monitored. In the last two

days, mice had a free choice between two bottles, one with sucrose (1 % in tap water) and another with the sole water. The position of bottles was switched every 24 h to avoid bias due to side preferences. Each day, bottles were weighed to determine intake level. Sucrose preference was defined as an average sucrose consumption level of 75 % or higher. The sucrose preference was calculated as a percentage of the sucrose solution on the total fluid intake during the 24h. Mice that showed a sucrose preference of 65% or below were considered anhedonic (Strekalova et al., 2006).

#### **2.2.6. Tail suspension test.**

The tail suspension test is a behavioral test used to evaluate depressive-like state in mice. The test was conducted as previously described (Steru et al., 1985). Before the test, mice were placed to the testing room for new environment habituation (at least 1 h before testing), then were individually suspended at 35 cm above the table top on a suspension bar, using a paper adhesive tape placed approximately 1 cm from the tip of the tail. Mice were suspended for 6 min and the immobility duration was recorded by a video camera. The time spent in immobility was analyzed off line. Mice were considered immobile only when they hung passively and completely motionless.

#### **2.3. Electrophysiology.**

Coronal slices (thickness, 270  $\mu$ m) from Tm4sf2<sup>+/y</sup> and Tm4sf2<sup>-/y</sup> 40-60 days old male mice were prepared as previously described (Murru et al., 2017).

Slices containing the LHB were transferred to a recording chamber and perfused with artificial CSF (aCSF) at a rate of ~2 mL/min and at room temperature. Whole-cell patch-clamp electrophysiological recordings were performed with a Multiclamp 700B amplifier (Axon CNS Molecular Devices, USA) and using an infrared-differential interference contrast microscope (Nikon Eclipse FN1). Patch electrodes (borosilicate capillaries with a filament and an outer diameter of 1.5  $\mu$ m; Sutter Instruments) were prepared with a four-step horizontal puller (Sutter Instruments) and had a resistance of 3–5 M $\Omega$ . Voltage- and Current-clamp experiments were performed using an intracellular solution containing (in mM): 126 K-gluconate, 4 NaCl, 1 EGTA, 1 MgSO<sub>4</sub>, 0.5 CaCl<sub>2</sub>, 3 ATP (magnesium salt), 0.1 GTP (sodium salt), 10 glucose, and 10 HEPES–KOH (pH 7.28), and as external solution a standard aCSF containing (in mM): 125 NaCl, 2.5 KCl, 1.25 NaH<sub>2</sub>PO<sub>4</sub>, 1 MgCl<sub>2</sub>, 2 CaCl<sub>2</sub>, 25 glucose, and mM NaHCO<sub>3</sub> (pH 7.3), if not stated otherwise. The analysis of basal neuronal firing patterns were conducted at resting membrane potential (RMP) in whole-cell configuration according to

the literature (Weiss and Veh, 2011). To evaluate LHb neurons active and passive membrane properties, a series of depolarizing current steps (0-180 pA) were injected (20 pA per step, 1 s duration) to evoke AP firing. The AP frequency was correlated to the current injected in an input/output (I/O) curve. The AP accommodation has been calculated dividing the duration of the current step in ten bins and counting AP for each bin to obtain the instantaneous firing frequency. AP feature analysis were performed for the first and the last AP evoked by 100 pA current injection. Miniature excitatory and inhibitory post-synaptic currents (mEPSCs/mIPSCs) were recorded as previously described (Pizzamiglio et al., 2016). GABA<sub>B</sub>-GIRK currents were recorded in whole-cell voltage clamp configuration in presence of bicuculline (20  $\mu$ M) and kynurenic acid (3 mM) to block GABA<sub>A</sub> and glutamatergic transmission respectively. GIRK currents were measured (at -50 mV holding potential) and were evoked by bath application of GABA<sub>B</sub> agonist baclofen (100  $\mu$ M) and confirmed by antagonism with 1 mM Ba<sup>2+</sup>, a selective inhibitor of inward rectifiers K<sup>+</sup> channels. Voltage-clamp recordings of voltage-gated Na<sup>+</sup> currents (VGNC) were performed using standard aCSF supplemented with bicuculline (20  $\mu$ M), kynurenic acid (3 mM) and Cadmium (100  $\mu$ M) to block GABA<sub>A</sub> receptors, glutamatergic transmission and voltage-gated Ca<sup>2+</sup> channels, respectively. Capillaries were filled with an internal solution containing (in mM): 140 CsCl, 2 MgCl<sub>2</sub>, 1 CaCl<sub>2</sub>, 10 EGTA, 10 HEPES-CsOH, 2 ATP (disodium salt, pH 7.3 with CsOH). VGNC were elicited by 5 mV steps (10 ms) from -50 to +70 mV and neurons were held at -40 mV. VGNC inactivation curves were constructed by recording the peak currents amplitude evoked by 20 ms test pulses to -20 mV, after 100 ms pre-pulses to potentials over the range of -80 to 25 mV (5 mV steps). Voltage-gated K<sup>+</sup> channels mediated currents (VGKC) were recorded using aCSF as for VGNC. Total VGKC ( $K_{total}$ ) were evoked through 10 mV voltage steps (1s, from -50 to +40 mV) preceded by 500 ms hyperpolarization pre-pulse (from -50 to -100mV) while sustained VGKC (D-type) were evoked inactivating the transient component (A-type) by using a 30 mV depolarizing pre-pulse step (from -50 to -20 mV). The A-type current was obtained by digital subtraction of the D-type from the  $K_{total}$ . VGKC inactivation curve were constructed by recording the currents peak amplitude evoked by 250 ms to +40 mV after 1.5 s pre-pulses to potentials over the range of -110 to 80 mV (10 mV steps). VGNC and VGKC peak currents were expressed through current density obtained dividing the peak current with neuron capacitance.



Currents were amplified, filtered at 5 kHz and digitized at 20 kHz. All the analyses were performed offline with Clampfit 10.1 software.

#### 2.4. Real-Time PCR.

mRNA from Tspan7<sup>+/y</sup> and Tspan7<sup>-/y</sup> hippocampi and habenulae was extracted using Nucleozol reagent following manufacturer instructions (Macherey Nagel). 1.5 µg of extracted mRNA was used to synthesize cDNA using SuperScript VILO cDNA Synthesis Kit (Thermo Fisher).

TSPAN7 and  $\alpha$ -actin (endogenous control) were amplified from 60 ng of cDNA in the presence of SYBR Green PCR Master Mix (Applied Biosystems), using Applied Biosystems 7000 Real-Time thermocycler. Primer sequences were as follows TSPAN7 Fw (ACCAGTTTTATGGAGACTAACATGG), TSPAN7 Rev (ATGCGCATGCCAATCAACT),  $\alpha$ -actin Fw (AGATGACCCAGATCATGTTTGAGA),  $\alpha$ -actin Rev (CCTCGTAGATGGGCACAGTGT).

Each sample was run in triplicate, and the results were calculated using the  $\Delta\Delta$ CT method to allow the normalization of each sample to the internal standard and comparison with the calibrator.

#### 2.5. Western Blot.

For the analyses of activated ERK, habenulae from Tm4sf2<sup>+/y</sup> and Tm4sf2<sup>-/y</sup> mice were dissected and homogenized in RIPA modified buffer (20 mM Tris, 150 mM NaCl, 1 mM EDTA, 1% NP40, 1% Triton X-100, protease inhibitors, pH 7.5).

For the analyses of ion channels, habenulae from Tm4sf2<sup>+/y</sup> and Tm4sf2<sup>-/y</sup> mice were dissected and membrane protein concentrated. Briefly, tissues were lysed in 10 volumes of homogenization buffer (0.32 M sucrose, 10 mM HEPES pH 7.4, 2 mM EDTA, protease inhibitors) and centrifuged at 1000 rpm for 10 min at 4°C. Supernatants were centrifuged at 50,000 rpm for 30 min at 4°C and the pellet re-suspended in homogenization buffer. Centrifugation was repeated for 15 min to yield crude membrane pellet. Pellet was re-suspended in RIPA modified buffer.

For each sample, 30 µg of proteins were loaded into polyacrylamide gel for western blotting analyses. The following primary antibodies were used: NaV1.1 (Alomone Labs, 1:200), NaV1.6 (Sigma Aldrich, 1:200), Kv4.2 (Sigma Aldrich, 1:200),  $\alpha$ -tubulin (Sigma Aldrich, 1:40000),  $\alpha$ -ERK (Cell Signaling, 1:1000),  $\alpha$ -pERK (Cell Signaling, 1:1000).



Horseradish peroxidase-conjugated secondary antibodies (GE Healthcare) were used and results visualized with ChemiDoc XRS+ System (BioRad) and analyzed by the Image Lab software.

## 2.6. PKC Kinase Activity Assay.

To evaluate the Kinase activity of PKC, brain samples from *Tm4sf2<sup>+/-</sup>* and *Tm4sf2<sup>-/-</sup>* mice were homogenized in Lysis Buffer (20 mM MOPS, 50 mM  $\beta$ -glycerolphosphate, 50 mM sodium fluoride, 1 mM sodium orthovanadate, 5 mM EGTA, 2 mM EDTA, 1% NP40, 1 mM DTT, protease inhibitor) and analyzed by PKC Kinase Activity Assay Kit (Abcam), accordingly to manufacturer's instructions. Positive (purified active PKC) and negative controls were used. Each sample was loaded in triplicate. Samples absorbance was measured at 450 nm with microplate reader GloMax (Promega).

## 2.7. Statistical analysis.

The data are represented as mean  $\pm$  SEM. All statistical analyses were conducted using GraphPad Prism. The statistical tests used are *t*-test and repeated-measures (RM) two-way ANOVA. For the tube test only was used the Fisher's exact probability test. The specific statistical test used is listed within Results with "n" values indicating the number of neurons recorded and/or mice used.  $V_{1/2}$  values were obtained from Boltzmann fit of voltage dependence of activation or inactivation of GNC and VGKC. For statistical significance, *p* values <0.05 were used.

## 3. Results

### 3.1. *Tm4sf2<sup>-/-</sup>* mice display ASD-like behaviors

Patients with mutations in *TM4SF2* gene have been often diagnosed also for ASD (Piton et al., 2011). For this reason, we subjected *Tm4sf2<sup>-/-</sup>* mice to several tests in order to identify an ASD-like phenotype. Firstly, we analyzed *Tm4sf2<sup>+/-</sup>* and *Tm4sf2<sup>-/-</sup>* mice for repetitive and stereotyped behaviors through self-grooming and marble-burying tests. *Tm4sf2<sup>-/-</sup>* mice displayed increased self-grooming behavior in terms of self-grooming episodes and duration (Fig. 1 A) (Self-grooming episodes (N°): *Tm4sf2<sup>+/-</sup>*:  $5.14 \pm 0.59$  vs *Tm4sf2<sup>-/-</sup>*:  $15.33 \pm 1.36$ , \*\*\**P*<0.001 unpaired *t*-test; Self-grooming duration (s): *Tm4sf2<sup>+/-</sup>*:  $68.71 \pm 7.43$  vs *Tm4sf2<sup>-/-</sup>*:  $129.90 \pm 12.50$ , \*\**P*<0.01 unpaired *t*-test; *n*<sub>mice</sub>= 7-12) and buried less marbles with an increased latency (Fig. 1 B, C) (buried marbles (N°): *Tm4sf2<sup>+/-</sup>*:  $5.67 \pm 2.06$  vs *Tm4sf2<sup>-/-</sup>*:  $1.75 \pm 0.52$ , \**P*<0.05 unpaired *t*-test; latency (s): *Tm4sf2<sup>+/-</sup>*:  $165.30 \pm 21.92$  vs *Tm4sf2<sup>-/-</sup>*:  $495.40 \pm 99.22$ , \**P*<0.05 unpaired *t*-test; *n*<sub>mice</sub>= 6-12). Moreover, the social dominance of *Tm4sf2<sup>+/-</sup>* and

Tm4sf2<sup>-/-</sup> mice, evaluated by using the tube test, was equal between genotypes (Fig. 1 D, E) (percentage of wins (%): Tm4sf2<sup>+/+</sup>: 44 vs Tm4sf2<sup>-/-</sup>: 56;  $n_{\text{mice}} = 6-12$ ,  $P > 0.05$  Fisher's exact probability test).

Next, Tm4sf2<sup>+/+</sup> and Tm4sf2<sup>-/-</sup> mice were evaluated for social behavior through the 3-chamber sociability test (Fig. 1 F). The 3-chamber test is widely used to assess sociability in rodents, taking advantage of the natural mice inclination in spending more time with another rodent (sociability) than with an inanimate object. The mouse was tested in a three-chambered box with openings between the chambers. At first, a stranger mouse was placed inside a small cage in the left chamber, while an empty cage (the object) was positioned in the right one. The time spent investigating (sniffing) the target mouse or the object was continuously scored for 10 min. Tm4sf2<sup>-/-</sup> mice spent equal time investigating the stranger mouse and the object compared to Tm4sf2<sup>+/+</sup> mice (Fig. 1 G) (time sniffing object (s): Tm4sf2<sup>+/+</sup>:  $77.53 \pm 8.13$  vs Tm4sf2<sup>-/-</sup>:  $92.94 \pm 9.41$ ; time sniffing mouse (s): Tm4sf2<sup>+/+</sup>:  $116.90 \pm 12.67$  vs Tm4sf2<sup>-/-</sup>:  $89.66 \pm 7.20$ ;  $n_{\text{mice}} = 12-14$ ,  $*P < 0.05$  unpaired *t*-test), suggesting an impaired social behavior. Social relationship in mammals is a highly rewarding experience, and the anhedonia for social interaction is one of the symptoms experienced by ASD patients (Chevallier et al., 2012a; Novacek et al., 2016). To evaluate the capacity of Tm4sf2<sup>-/-</sup> mice to experience pleasure, we used the two-bottle choice paradigm, where mice were trained to drink water or water with 1% sucrose (Fig. 1 H). Naturally, rodents display a preference for 1% sucrose respect to the sole water. Tm4sf2<sup>-/-</sup> mice showed a significant reduction in the sucrose preference (Fig. 1 I) (Sucrose preference 1st day (%): Tm4sf2<sup>+/+</sup>:  $78.53 \pm 3.79$  vs Tm4sf2<sup>-/-</sup>:  $62.02 \pm 6.44$ ,  $*P < 0.05$  unpaired *t*-test; Sucrose preference 2nd day (%): Tm4sf2<sup>+/+</sup>:  $84.10 \pm 2.78$  vs Tm4sf2<sup>-/-</sup>:  $62.87 \pm 5.98$ ,  $**P < 0.01$  unpaired *t*-test;  $n_{\text{mice}} = 7$  per group) despite an equal fluid intake during the task (Fig. 1 L) (Fluid intake (mL): Tm4sf2<sup>+/+</sup>:  $n_{\text{mice}} = 7$  vs Tm4sf2<sup>-/-</sup>:  $n_{\text{mice}} = 7$   $P > 0.05$  two-way ANOVA RM,  $F_{(5,60)} = 1.22$ ). This data demonstrated that Tm4sf2<sup>-/-</sup> mice are anhedonic compared to Tm4sf2<sup>+/+</sup> mice. Finally, to evaluate a possible depressive-like state, we subjected Tm4sf2<sup>+/+</sup> and Tm4sf2<sup>-/-</sup> mice to the tail suspension test (Fig. 1 M) and we found a depressive-like behavior in Tm4sf2<sup>-/-</sup> compared to Tm4sf2<sup>+/+</sup> mice (Fig. 1 N) (Immobility (s): Tm4sf2<sup>+/+</sup>:  $107.70 \pm 7.70$  vs Tm4sf2<sup>-/-</sup>:  $134.20 \pm 6.76$ ;  $n_{\text{mice}} = 11-13$ ,  $*P < 0.05$  unpaired *t*-test). Taken together, these results demonstrated that Tm4sf2<sup>-/-</sup> mice show ASD-like behaviors.

Fig. 1: Tm4sf2<sup>-/-</sup> mice show ASD-like behaviors A) Quantification histograms showing an increased Self-Grooming behavior in terms of sel-grooming episodes and time in Tm4sf2<sup>-/-</sup> mice compared to Tm4sf2<sup>+/+</sup> animals; B) Scheme of the marble burying test; C) Quantification of the mice performance in the marble burying test. Tm4sf2<sup>-/-</sup> mice buried less marbles with an increased latency compared to Tm4sf2<sup>+/+</sup> mice; D) Representation of the tube test for assessing aggressive behavior in mice; E) Histograms showing no changes in aggressive behaviors between genotypes; F) Scheme representing the Three-chambers sociability test for mice social behavior; G) Quantification of social behavior in Tm4sf2<sup>+/+</sup> and Tm4sf2<sup>-/-</sup> mice. Tm4sf2<sup>-/-</sup> mice showed decreased sociability compared to Tm4sf2<sup>+/+</sup> mice; H) Sucrose preference test scheme for assessing anhedonia in mice; I) Quantification of sucrose preference showing anhedonic behavior in Tm4sf2<sup>-/-</sup> mice compared to Tm4sf2<sup>+/+</sup> animals; L) Quantification of fluid intake of Tm4sf2<sup>+/+</sup> and Tm4sf2<sup>-/-</sup> mice; M) Scheme of the tail suspension test used to assess depressive-like state in mice; N) Histogram showing an increased immobility of Tm4sf2<sup>-/-</sup> compared to Tm4sf2<sup>+/+</sup> mice suggesting a depressive-like behavior.

### 3.2. Altered LHb neuronal firing pattern in Tm4sf2<sup>-/-</sup> mice

Recently, the LHb has been described as an important brain area in coordinating several brain regions involved in cognitive-related behaviors and we found that TSPAN7 is expressed in the mouse habenula (Fig. 2 A, B). Therefore, we evaluated whether TSPAN7 absence affects LHb neuronal activity in Tm4sf2<sup>-/-</sup> mice. We analyzed LHb glutamatergic neurons given their predominance respect to the GABAergic ones (Lecca et al., 2014) and for their involvement in psychiatric disorders (Meyer et al., 2015; Lecca et al., 2016; Tchenio et al., 2017; Li et al., 2019; Valentinova et al., 2019). Since TSPAN7 is an important player in AMPA receptors trafficking in hippocampus (Muller et al., 2017), we recorded mEPSCs from LHb glutamatergic neurons. Surprisingly, we did not find alterations nor in frequency neither in amplitude of mEPSCs between genotypes (Fig. 2 C, D) (mEPSCs Amplitude (pA): Tm4sf2<sup>+/+</sup>:  $15.40 \pm 1.26$  vs Tm4sf2<sup>-/-</sup>:  $14.62 \pm 1.81$ ; mEPSCs Frequency (pA): Tm4sf2<sup>+/+</sup>:  $1.69 \pm 0.37$  vs Tm4sf2<sup>-/-</sup>:  $1.38 \pm 0.36$ ;  $n_{\text{neurons}} = 5-7$ ,  $n_{\text{mice}} = 3$ ;  $P > 0.05$  unpaired *t*-test). Additionally, we analyzed inhibitory inputs onto LHb neurons recording mIPSCs and GABA<sub>B</sub>-mediated GIRK potassium currents. Also in this case no changes have been detected in Tm4sf2<sup>-/-</sup> mice (Fig. 2 E-H) (mIPSCs Amplitude (pA): Tm4sf2<sup>+/+</sup>:  $23.35 \pm 1.82$  vs Tm4sf2<sup>-/-</sup>:  $32.95 \pm 4.65$ ; mIPSCs Frequency (pA): Tm4sf2<sup>+/+</sup>:  $1.15 \pm 0.12$  vs Tm4sf2<sup>-/-</sup>:  $0.86 \pm 0.12$ ;  $n_{\text{neurons}} = 8-18$ ,  $n_{\text{mice}} = 3-4$ ;  $P > 0.05$  unpaired *t*-test; GABA<sub>B</sub>-GIRK currents (pA): Tm4sf2<sup>+/+</sup>:  $64.43 \pm 10.21$  vs Tm4sf2<sup>-/-</sup>:  $54.09 \pm 12.05$ ;  $n_{\text{neurons}} = 11-14$ ,  $n_{\text{mice}} = 4$ ;  $P > 0.05$  unpaired *t*-test).

Fig. 2: Tm4sf2<sup>-/-</sup> mice LHb neurons show normal synaptic inputs A) Cartoon showing a coronal brain slice containing the hippocampus and the habenula; B) Histogram showing the TSPAN7 mRNA relative expression in mice habenula normalized on hippocampus; C) Representative traces of mEPSCs recorded from Tm4sf2<sup>+/+</sup> and Tm4sf2<sup>-/-</sup> mice LHb neurons; D) Quantification of mEPSCs amplitude and frequency recorded from Tm4sf2<sup>+/+</sup> and Tm4sf2<sup>-/-</sup> mice LHb neurons; E)

Representative traces of mIPSCs recorded from Tm4sf2<sup>+/y</sup> and Tm4sf2<sup>-/-</sup> mice LHB neurons; F) Quantification of mIPSCs amplitude and frequency recorded from Tm4sf2<sup>+/y</sup> and Tm4sf2<sup>-/-</sup> mice LHB neurons; G) Representative traces of Baclofen-evoked GABA<sub>B</sub>-GIRK currents recorded from Tm4sf2<sup>+/y</sup> and Tm4sf2<sup>-/-</sup> mice LHB neurons; H) Quantification of Baclofen-evoked GABA<sub>B</sub>-GIRK currents recorded from Tm4sf2<sup>+/y</sup> and Tm4sf2<sup>-/-</sup> mice LHB neurons

LHB glutamatergic neurons show four different firing patterns, namely tonic regular, tonic irregular, silent and burst (Weiss and Veh, 2011). Interestingly, we found that Tm4sf2<sup>-/-</sup> mice present a strong reduction in the number of LHB tonic regular firing neurons and a concomitant significant increase in the number of silent neurons with respect to Tm4sf2<sup>+/y</sup> mice. Noteworthy, even if not statistically significant, we noticed that tonic irregular firing neurons almost doubled in Tm4sf2<sup>-/-</sup> mice respect to Tm4sf2<sup>+/y</sup> mice (Fig. 3 A-E) (LHB tonic regular firing neurons (%): Tm4sf2<sup>+/y</sup>: 45.77 ± 8.30 vs Tm4sf2<sup>-/-</sup>: 12.29 ± 3.45, \*\**P*<0.01 unpaired *t*-test; LHB tonic irregular firing neurons (%): Tm4sf2<sup>+/y</sup>: 17.32 ± 4.94 vs Tm4sf2<sup>-/-</sup>: 33.87 ± 8.75; LHB silent neurons (%): Tm4sf2<sup>+/y</sup>: 23.16 ± 6.10 vs Tm4sf2<sup>-/-</sup>: 43.04 ± 6.41, \*\**P*<0.01 unpaired *t*-test; LHB burst firing neurons (%): Tm4sf2<sup>+/y</sup>: 13.72 ± 5.55 vs Tm4sf2<sup>-/-</sup>: 10.80 ± 4.97; *n*<sub>neurons</sub>= 64-68, *n*<sub>mice</sub>= 10-14). Additionally, we analyzed the resting membrane potential (RMP) for neurons belonging to each category and we did not find differences between genotypes (Fig. 3 F) (LHB tonic regular RMP (mV): Tm4sf2<sup>+/y</sup>: -47.13 ± 1.17 vs Tm4sf2<sup>-/-</sup>: -47.64 ± 1.54; LHB tonic irregular RMP (mV): Tm4sf2<sup>+/y</sup>: -44.54 ± 1.77 vs Tm4sf2<sup>-/-</sup>: -46.95 ± 0.94; LHB silent RMP (mV): Tm4sf2<sup>+/y</sup>: -51.47 ± 1.25 vs Tm4sf2<sup>-/-</sup>: -53.79 ± 1.18; LHB burst RMP (mV): Tm4sf2<sup>+/y</sup>: -57.25 ± 1.82 vs Tm4sf2<sup>-/-</sup>: -54.98 ± 1.26; *n*<sub>neurons</sub>= 64-68, *n*<sub>mice</sub>= 10-14, unpaired *t*-test). All together, these results demonstrated that TSPAN7 absence affects LHB neuronal firing pattern.

Fig. 3: Tm4sf2<sup>-/-</sup> mice LHB neurons show altered firing pattern A-D) Representative traces of LHB neuronal firing pattern, namely tonic regular and irregular firing, silent and burst firing neurons. The resting membrane potential of the recorded neuron is stated on the left; E) Pie charts showing the percentage of Tm4sf2<sup>+/y</sup> and Tm4sf2<sup>-/-</sup> mice LHB neurons based on firing behavior in A-D); F) Analysis of the LHB neurons resting membrane potential (RMP) divided for the categories in E).

### 3.3. Altered LHB neuronal excitability and AP features in Tm4sf2<sup>-/-</sup> mice

Afterwards, we analyzed AP basal firing at RMP concentrating our attention in tonic regular, irregular and bursting neurons since the silent ones are not active at RMP. We found a decreased AP firing frequency in Tm4sf2<sup>-/-</sup> mice compared to Tm4sf2<sup>+/y</sup> mice (Fig. 4 A, B) (AP frequency (Hz): Tm4sf2<sup>+/y</sup>: 6.96 ± 0.83 vs Tm4sf2<sup>-/-</sup>: 3.67 ± 0.46; *n*<sub>neurons</sub>= 36-55, *n*<sub>mice</sub>= 10;

\*\*\* $P < 0.001$  unpaired  $t$ -test). In accordance, current-clamp experiments showed a huge decrease in AP firing frequency upon depolarizing current injection at the majority of current steps tested (AP frequency (Hz): Tm4sf2<sup>+/y</sup>:  $n_{\text{neurons}} = 32$  vs Tm4sf2<sup>-y</sup>:  $n_{\text{neurons}} = 41$  \*\*\* $P < 0.001$  two-way ANOVA RM,  $F_{(1;639)} = 16.57$ ;  $n_{\text{mice}} = 6-8$ ), and strong AP frequency accommodation in Tm4sf2<sup>-y</sup> mice (Fig. 4 C-E) (AP instantaneous frequency (Hz): Tm4sf2<sup>+/y</sup>:  $n_{\text{neurons}} = 32$  vs Tm4sf2<sup>-y</sup>:  $n_{\text{neurons}} = 41$  \*\* $P < 0.01$  two-way ANOVA RM,  $F_{(1;630)} = 13.12$ ;  $n_{\text{mice}} = 6-8$ ). To study more in details neuronal excitability, we analyzed also the features of the first and the last AP evoked by the 1 s injection of 100 pA depolarizing current (Fig. 4 F). This analysis showed no changes for AP threshold between genotypes (Fig. 4 G) (1st AP threshold (mV): Tm4sf2<sup>+/y</sup>:  $-35.44 \pm 1.41$  vs Tm4sf2<sup>-y</sup>:  $-35.63 \pm 0.92$ ; last AP threshold (mV): Tm4sf2<sup>+/y</sup>:  $-30.38 \pm 1.26$  vs Tm4sf2<sup>-y</sup>:  $-28.76 \pm 1.02$ ;  $n_{\text{neurons}} = 32-40$ ,  $n_{\text{mice}} = 6-8$ ;  $P > 0.05$  unpaired  $t$ -test), while AP amplitude decreased only for the last AP evoked in Tm4sf2<sup>-y</sup> mice (Fig. 4 H) (1st AP amplitude (mV): Tm4sf2<sup>+/y</sup>:  $63.98 \pm 2.17$  vs Tm4sf2<sup>-y</sup>:  $62.58 \pm 1.77$ ,  $P > 0.05$  unpaired  $t$ -test; last AP amplitude (mV): Tm4sf2<sup>+/y</sup>:  $53.41 \pm 1.99$  vs Tm4sf2<sup>-y</sup>:  $43.71 \pm 2.81$ , \*\* $P < 0.01$  unpaired  $t$ -test;  $n_{\text{neurons}} = 32-40$ ,  $n_{\text{mice}} = 6-8$ ). On the other hand, we highlighted an increased AP width in Tm4sf2<sup>-y</sup> mice (Fig. 4 I) (1st AP width (ms): Tm4sf2<sup>+/y</sup>:  $0.75 \pm 0.05$  vs Tm4sf2<sup>-y</sup>:  $0.94 \pm 0.06$ , \* $P < 0.05$  unpaired  $t$ -test; last AP width (ms): Tm4sf2<sup>+/y</sup>:  $-1.03 \pm 0.07$  vs Tm4sf2<sup>-y</sup>:  $2.47 \pm 0.37$ , \*\* $P < 0.01$  unpaired  $t$ -test,  $n_{\text{neurons}} = 32-40$ ,  $n_{\text{mice}} = 6-8$ ) that suggested alterations in AP kinetic. As expected, AP kinetic analysis showed a decreased maximum rise (1st AP maximum rise slope (mV/ms): Tm4sf2<sup>+/y</sup>:  $221.20 \pm 13.83$  vs Tm4sf2<sup>-y</sup>:  $178.20 \pm 10.18$ , \* $P < 0.05$  unpaired  $t$ -test; last AP maximum rise slope (mV/ms): Tm4sf2<sup>+/y</sup>:  $140.40 \pm 11.06$  vs Tm4sf2<sup>-y</sup>:  $87.11 \pm 12.21$ , \*\* $P < 0.01$  unpaired  $t$ -test;  $n_{\text{neurons}} = 32-40$ ,  $n_{\text{mice}} = 6-8$ ) and maximum decay slope (1st AP maximum decay slope (mV/ms): Tm4sf2<sup>+/y</sup>:  $119.50 \pm 8.71$  vs Tm4sf2<sup>-y</sup>:  $96.67 \pm 7.22$ , \* $P < 0.05$  unpaired  $t$ -test; last AP maximum decay slope (mV/ms): Tm4sf2<sup>+/y</sup>:  $86.61 \pm 6.71$  vs Tm4sf2<sup>-y</sup>:  $60.58 \pm 8.03$ , \* $P < 0.05$  unpaired  $t$ -test;  $n_{\text{neurons}} = 32-40$ ,  $n_{\text{mice}} = 6-8$ ) in Tm4sf2<sup>-y</sup> mice for the first and the last AP evoked (Fig. 4 L, M). Collectively, these results suggested a reduced excitability and slower AP kinetics of Tm4sf2<sup>-y</sup> mice LHb neurons.

Fig. 4: Decreased excitability and altered AP features of LHb Tm4sf2<sup>-y</sup> mice neurons A) Representative traces showing the spontaneous firing activity of Tm4sf2<sup>+/y</sup> and Tm4sf2<sup>-y</sup> mice LHb neurons; B) Quantification of AP firing frequency; C) Representative traces of AP evoked by 100 pA of injected current in current-clamp mode. Under the traces you can find the depolarizing current step used; D) Analysis of AP frequency for each current step used during the current-clamp experiment; E) Quantification of the instantaneous AP frequency induced by 100 pA of injected current. You can see the prominent AP accommodation showed by Tm4sf2<sup>-y</sup> compared Tm4sf2<sup>+/y</sup> mice; F) Representative trace of the first and the last AP evoked by 100 pA of current injection in Tm4sf2<sup>+/y</sup> and Tm4sf2<sup>-y</sup> mice LHb neurons; Quantification histograms for G) AP thresholds,

H) AP amplitudes, I) AP half-widths, L) Maximum rise slopes, M) Maximum decay slopes of the first and the last AP evoked by 100pA of current injection in Tm4sf2<sup>+/y</sup> and Tm4sf2<sup>-/-</sup> Lhb mice neurons.

### 3.4. Tonic firing neurons are the mainly affected for neuronal excitability and AP features in Tm4sf2<sup>-/-</sup> mice

Since we noticed an altered firing pattern of Tm4sf2<sup>-/-</sup> mice Lhb neurons, we repeated the current-clamp experiment at the light of firing pattern neuronal categories. In accordance with the previous experiment (Fig. 4 C, D), we found a significant reduction in AP firing frequency of Lhb tonic regular firing and silent neurons and a downtrend, even if not significant, for tonic irregular neurons in Tm4sf2<sup>-/-</sup> mice (Fig. 5 A-C) (AP frequency tonic regular neurons (Hz): Tm4sf2<sup>+/y</sup>:  $n_{\text{neurons}} = 15$  vs Tm4sf2<sup>-/-</sup>:  $n_{\text{neurons}} = 9$  \*\*\* $P < 0.001$  two-way ANOVA RM,  $F_{(1;207)} = 9.95$ ;  $n_{\text{mice}} = 7-9$ ; AP frequency tonic irregular neurons (Hz): Tm4sf2<sup>+/y</sup>:  $n_{\text{neurons}} = 4$  vs Tm4sf2<sup>-/-</sup>:  $n_{\text{neurons}} = 9$   $P > 0.05$  two-way ANOVA RM,  $F_{(1;99)} = 1.096$   $n_{\text{mice}} = 7-9$ ; AP frequency silent neurons (Hz): Tm4sf2<sup>+/y</sup>:  $n_{\text{neurons}} = 6$  vs Tm4sf2<sup>-/-</sup>:  $n_{\text{neurons}} = 11$   $P < 0.05$  two-way ANOVA RM,  $F_{(1;117)} = 6.23$ ;  $n_{\text{mice}} = 7-9$ ). Furthermore, we analyzed the AP features of the first AP evoked by 100 pA of current injection for each category. Interestingly, we found no changes for AP threshold and amplitude in Tm4sf2<sup>-/-</sup> mice (Fig. 5 D-E), while AP half-width increased in tonic regular and irregular Lhb neurons (Fig. 5 F) (1st AP width tonic regular (ms): Tm4sf2<sup>+/y</sup>:  $0.62 \pm 0.06$  vs Tm4sf2<sup>-/-</sup>:  $1.03 \pm 0.12$ , \*\* $P < 0.01$  unpaired  $t$ -test,  $n_{\text{neurons}} = 9-16$ ,  $n_{\text{mice}} = 7-9$ ; 1st AP width tonic irregular (ms): Tm4sf2<sup>+/y</sup>:  $0.58 \pm 0.11$  vs Tm4sf2<sup>-/-</sup>:  $1.06 \pm 0.05$ , \*\*\* $P < 0.001$  unpaired  $t$ -test,  $n_{\text{neurons}} = 4-9$ ,  $n_{\text{mice}} = 7-9$ ). Concerning AP kinetic, in Tm4sf2<sup>-/-</sup> mice we noticed a reduction in the rise and decay slopes of tonic irregular neurons while tonic regular neurons displayed a downtrend for the rise slope and a significant reduction for the decay slope (Fig. 5 G, H) (AP maximum rise slope tonic regular neurons (mV/ms): Tm4sf2<sup>+/y</sup>:  $235.10 \pm 18.49$  vs Tm4sf2<sup>-/-</sup>:  $188.40 \pm 21.97$ ,  $P > 0.05$  unpaired  $t$ -test,  $n_{\text{neurons}} = 9-17$ ,  $n_{\text{mice}} = 7-9$ ; AP maximum decay slope tonic regular neurons (mV/ms): Tm4sf2<sup>+/y</sup>:  $140.40 \pm 13.87$  vs Tm4sf2<sup>-/-</sup>:  $93.58 \pm 15.47$ , \* $P < 0.05$  unpaired  $t$ -test,  $n_{\text{neurons}} = 9-17$ ,  $n_{\text{mice}} = 7-9$ ; AP maximum rise slope tonic irregular neurons (mV/ms): Tm4sf2<sup>+/y</sup>:  $233.90 \pm 27.59$  vs Tm4sf2<sup>-/-</sup>:  $140.30 \pm 11.47$ , \*\* $P < 0.01$  unpaired  $t$ -test,  $n_{\text{neurons}} = 4-9$ ,  $n_{\text{mice}} = 7-9$ ; AP maximum decay slope tonic irregular neurons (mV/ms): Tm4sf2<sup>+/y</sup>:  $134.20 \pm 25.13$  vs Tm4sf2<sup>-/-</sup>:  $73.47 \pm 4.92$ , \*\* $P < 0.01$  unpaired  $t$ -test,  $n_{\text{neurons}} = 4-9$ ,  $n_{\text{mice}} = 7-9$ ).



Collectively, these results highlighted altered AP firing frequency and kinetic in Tm4sf2<sup>-/-</sup> mice, indicating tonic regular and irregular neurons as the mainly affected categories in Tm4sf2<sup>-/-</sup> mice.

Fig. 5: Decreased excitability and altered AP features of LHB Tm4sf2<sup>-/-</sup> mice neurons A-C) Analysis of AP frequency for each current step used during the current-clamp experiment for tonic regular, irregular and silent neurons; Quantification histograms for D) AP thresholds, E) AP amplitudes, F) AP half-widths, G) Maximum rise slopes, H) Maximum decay slopes of the first AP evoked by 100pA of current injection in Tm4sf2<sup>+/+</sup> and Tm4sf2<sup>-/-</sup> LHB mice neurons.

### 3.5. Tm4sf2<sup>-/-</sup> mice display altered sodium and potassium voltage-gated channel function in LHB neurons

Sodium and potassium voltage-gated channels (VGNC and VGKC, respectively) are key players in regulating neuronal excitability (Goldman et al., 2001; Hill, 2001; Miles et al., 2010; Amendola et al., 2012; Lin et al., 2019). For this reason, we analyzed VGNC and VGKC function in LHB neurons of Tm4sf2<sup>-/-</sup> mice. Applying classic voltage-clamp protocols (Fig. 4 A) we found that Tm4sf2<sup>-/-</sup> mice LHB neurons displayed a strong reduction in the total VGNC-mediated current (VGNC current density (pA/pF): Tm4sf2<sup>+/+</sup>:  $n_{\text{neurons}} = 12$  vs Tm4sf2<sup>-/-</sup>:  $n_{\text{neurons}} = 15$  \*\*\* $P < 0.001$  two-way ANOVA RM,  $F_{(2, 500)} = 5.44$ ;  $n_{\text{mice}} = 3$  per group) and a delay in their activation ( $V_{1/2}$  (mV): Tm4sf2<sup>+/+</sup>:  $-33.13 \pm 0.82$  vs Tm4sf2<sup>-/-</sup>:  $-27.75 \pm 0.93$   $n_{\text{neurons}} = 12-15$ ,  $n_{\text{mice}} = 3$ ; \*\*\* $P < 0.001$  unpaired  $t$ -test) and inactivation kinetic ( $V_{1/2}$  (mV): Tm4sf2<sup>+/+</sup>:  $-48.69 \pm 0.31$  vs Tm4sf2<sup>-/-</sup>:  $-45.79 \pm 0.42$   $n_{\text{neurons}} = 12-15$ ,  $n_{\text{mice}} = 3$ ; \*\*\* $P < 0.001$  unpaired  $t$ -test) with respect to Tm4sf2<sup>+/+</sup> mice (Fig. 4 B-G). Interestingly, we found that VGKCs were regulated in the opposite fashion with respect to VGNCs in Tm4sf2<sup>-/-</sup> mice. Indeed, an increase in the total current ( $K_{\text{total}}$ ) in Tm4sf2<sup>-/-</sup> mice LHB neurons has been noticed (Fig. 4 H-L) (VGKC current density (pA/pF): Tm4sf2<sup>+/+</sup>:  $n_{\text{neurons}} = 11$  vs Tm4sf2<sup>-/-</sup>:  $n_{\text{neurons}} = 15$  \*\* $P < 0.05$  two-way ANOVA RM,  $F_{(9, 216)} = 3.51$ ;  $n_{\text{mice}} = 3-4$ ). Moreover, being VGKC classified as non-inactivating delayed rectifiers (D-type) or rapidly activating/inactivating channels (A-type), we decided to investigate both of them. We applied a specific voltage-clamp protocol in order to inactivate the A-type component and record exclusively the D-type. After a digital subtraction, we extrapolated and analyzed the A-type component and we found it increased in Tm4sf2<sup>-/-</sup> mice LHB neurons (A-type current density (pA/pF): Tm4sf2<sup>+/+</sup>:  $n_{\text{neurons}} = 11$  vs Tm4sf2<sup>-/-</sup>:  $n_{\text{neurons}} = 15$  \*\*\* $P < 0.001$  two-way ANOVA RM,  $F_{(9, 207)} = 6.90$ ;  $n_{\text{mice}} = 3-4$ ), while the D-type were unaffected (Fig. 4 M-R) (D-type current density (pA/pF): Tm4sf2<sup>+/+</sup>:  $n_{\text{neurons}} = 11$  vs Tm4sf2<sup>-/-</sup>:  $n_{\text{neurons}} = 15$



$P > 0.05$  two-way ANOVA RM,  $F_{(9;216)} = 0.86$ ;  $n_{\text{mice}} = 3-4$ ). We also found that VGKC activated at more hyperpolarized potentials in Tm4sf2<sup>-/-</sup> compared to Tm4sf2<sup>+/+</sup> mice ( $V_{1/2}$  (mV): Tm4sf2<sup>+/+</sup>:  $-4.38 \pm 1.93$  vs Tm4sf2<sup>-/-</sup>:  $-19.18 \pm 6.76$   $n_{\text{neurons}} = 11-15$ ,  $n_{\text{mice}} = 3-4$ ;  $*P < 0.05$  unpaired  $t$ -test), with no change in inactivation kinetic (Fig. 4 S-V) ( $V_{1/2}$  (mV): Tm4sf2<sup>+/+</sup>:  $-10.80 \pm 2.16$  vs Tm4sf2<sup>-/-</sup>:  $-10.90 \pm 2.26$   $n_{\text{neurons}} = 11-15$ ,  $n_{\text{mice}} = 3-4$ ;  $P > 0.05$  unpaired  $t$ -test). Our results suggested that the alterations in LHB neuronal firing activity described in Tm4sf2<sup>-/-</sup> mice could be the effect of an aberrant voltage-gated ion channels (VGIC) function.

Fig. 6: Altered Na<sup>+</sup> and K<sup>+</sup> voltage-gated channels function and kinetic in Tm4sf2<sup>-/-</sup> mice LHB neurons compared to Tm4sf2<sup>+/+</sup> mice. A) Voltage step protocol used to evoke VGNC-mediated currents; B) Representative traces showing decreased VGNC-mediated currents in Tm4sf2<sup>-/-</sup> mice LHB neurons compared to Tm4sf2<sup>+/+</sup> mice; C) Quantification of VGNC-mediated current density from Tm4sf2<sup>+/+</sup> and Tm4sf2<sup>-/-</sup> mice; D) Voltage-dependence of activation for Tm4sf2<sup>+/+</sup> and Tm4sf2<sup>-/-</sup> mice VGNC. The lines are the best-fitted Boltzmann curves; E) Half-maximal voltage activation ( $V_{1/2}$ ) extrapolated from the curve fitting in D); F) Steady-state inactivation curves from VGNC-mediated currents recorded using the voltage protocol reported inset. The lines are the best-fitted Boltzmann curves; G) Half-maximal voltage for inactivation ( $V_{1/2}$ ) obtained from the curve fitting in F); H) Voltage step protocol used to record VGKC-mediated currents; I) Representative traces of VGKC-mediated total current ( $K_{\text{total}}$ ) recorded from Tm4sf2<sup>+/+</sup> and Tm4sf2<sup>-/-</sup> mice LHB neurons; L) Quantification of current density showing increased VGKC-mediated current in Tm4sf2<sup>-/-</sup> compared to Tm4sf2<sup>+/+</sup> mice; M) Voltage step protocol used to record currents mediated by non-inactivating delayed rectifiers VGKC (D-type); N, Representative traces of D-type currents recorded using the protocol in M); O) Quantification of current density showing no changes for non-inactivating delayed rectifiers VGKC-mediated (D-type) currents between genotypes; P) The A-type current has been obtained through digital subtraction of the D-type from the  $K_{\text{total}}$ ; Q) Representative A-type current traces obtained by digital subtraction in P); R) Quantification of current density showing increased A-type VGKC-mediated currents in Tm4sf2<sup>-/-</sup> compared to Tm4sf2<sup>+/+</sup> mice; S) Voltage-dependence of activation for Tm4sf2<sup>+/+</sup> and Tm4sf2<sup>-/-</sup> mice VGKC. The lines are the best-fitted Boltzmann curves; T) Half-maximal voltage activation ( $V_{1/2}$ ) extrapolated from the curve fitting in S); U) Steady-state inactivation curves from VGKC-mediated currents recorded using the voltage protocol reported inset. The lines are the best-fitted Boltzmann curves; V) Half-maximal voltage activation ( $V_{1/2}$ ) extrapolated from the curve fitting in U).

### 3.6. TSPAN7 loss of function alters VGNC expression and PKC-ERK signaling

Since our results pinpoint on ion channels altered expression in the LHB, we quantified by western blot the habenular expression levels of some VGNC and VGKC subunits in Tm4sf2<sup>+/+</sup> and Tm4sf2<sup>-/-</sup> mice. Interestingly, we found a significant reduction for Na<sub>v</sub>1.6 subunit expression in Tm4sf2<sup>-/-</sup> mice, while no alteration in VGNC Na<sub>v</sub>1.1 and VGKC Kv4.2 subunits have been detected (Fig. 5 A) (Na<sub>v</sub>1.1/ $\alpha$ -tubulin: Tm4sf2<sup>+/+</sup>:  $1.00 \pm 0.05$  vs Tm4sf2<sup>-/-</sup>:  $0.84 \pm 0.07$ ,  $n_{\text{mice}} = 3-5$ ;  $P > 0.05$  unpaired  $t$ -test with Welch's correction; Na<sub>v</sub>1.6/ $\alpha$ -tubulin: Tm4sf2<sup>+/+</sup>:  $1.00 \pm 0.15$  vs Tm4sf2<sup>-/-</sup>:  $0.61 \pm 0.04$ ,  $n_{\text{mice}} = 5-9$ ;  $P < 0.05$  unpaired  $t$ -test with Welch's correction; Kv4.2/ $\alpha$ -tubulin: Tm4sf2<sup>+/+</sup>:  $1.00 \pm 0.25$  vs Tm4sf2<sup>-/-</sup>:  $0.63 \pm 0.11$ ,  $n_{\text{mice}} = 4-6$ ;

$P > 0.05$  unpaired  $t$ -test with Welch's correction). Furthermore, we previously found that TSPAN7 modulates PICK1 function (Bassani et al., 2012; Murru et al., 2017) that, in turn, is involved in protein kinase C (PKC)-dependent regulation of ion channels (Hu et al., 2010). Therefore, we analyzed if the function of PKC and, one of its substrates, extracellular signal-regulated kinase (ERK), was affected by TSPAN7 absence in the LHb. Strikingly, we found that PKC and ERK were both hyperactivated in Tm4sf2<sup>-/-</sup> mice (Fig. 5 B, C) (PKC activity: Tm4sf2<sup>+/-</sup>:  $1.00 \pm 0.24$  vs Tm4sf2<sup>-/-</sup>:  $2.08 \pm 0.24$ ,  $n_{\text{mice}} = 6$  per group;  $**P < 0.01$  unpaired  $t$ -test; ERK activity (pERK/ERK): Tm4sf2<sup>+/-</sup>:  $1.00 \pm 0.06$  vs Tm4sf2<sup>-/-</sup>:  $1.15 \pm 0.02$ ,  $n_{\text{mice}} = 7$  per group;  $*P < 0.05$  unpaired  $t$ -test). These data demonstrated a decreased expression of VGNC and an increased PKC-ERK signaling that might lead to altered phosphorylation of VGNC and VGKC and, as final result, to an aberrant LHb neuronal firing pattern in Tm4sf2<sup>-/-</sup> compared to Tm4sf2<sup>+/-</sup> mice.

Fig. 7: Decreased VGNC expression and increased PKC and ERK activity in Tm4sf2<sup>-/-</sup> mice

A) Western blot of crude membrane preparation from Tm4sf2<sup>+/-</sup> and Tm4sf2<sup>-/-</sup> mice habenulae detected using ChemiDoc XRS+ System (BioRad) and quantification of voltage-gated sodium and potassium channel protein levels normalized on tubulin. You can see a downward trend and a significant reduced expression for Na<sub>v</sub>1.1 and Na<sub>v</sub>1.6 respectively in Tm4sf2<sup>-/-</sup> mice, while no changes for Kv4.2 has been detected; B) Quantification of PKC brain activity obtained using a PKC Kinase Activity Assay Kit showing a hyperactivity in Tm4sf2<sup>-/-</sup> compared to Tm4sf2<sup>+/-</sup> mice; C) Western blot of habenulae homogenates from Tm4sf2<sup>+/-</sup> and Tm4sf2<sup>-/-</sup> mice and quantification of expression levels represented as pERK/ERK ratio.  $\alpha$ -tubulin was used as loading control

#### 4. Discussion

This work stems from the evidence that *TM4SF2* gene mutations are correlated to ID and ASD (Piton et al., 2011; Bassani et al., 2013; Penzes et al., 2013). The comorbidity between ID and ASD is well documented with 10% of ID patients showing autistic features and 70% of autistic people presenting ID (Oeseburg et al., 2011; Schwartz and Neri, 2012). Consistently, we found an ID-like phenotype (Murru et al., 2017), decreased sociability and increased self-grooming. Unexpectedly, the marble-burying test showed a decrease in the number of marbles buried by Tm4sf2<sup>-/-</sup> mice compared to WT mice, while we expected an increase, coherently with a stereotypy-like behavior. This result could be explained by the propensity of Tm4sf2<sup>-/-</sup> mice in spending more time doing self-grooming, and/or by a reduced interest for the environment, similar to what ASD patients experience (Pierce and Courchesne, 2001;

Kawa and Pisula, 2010). Moreover, the marble-burying test has been also used to evaluate the anxiety-like behaviors in mice (Huang et al., 2018), then our data might also suggest reduced anxiety in *Tm4sf2<sup>-/-</sup>* mice. This is not the case, indeed we previously demonstrated no differences in the light and dark test (Murru et al., 2017), widely used to detect anxiety-like behaviors in mice (Hascoët et al., 2001; Liu et al., 2007; Huang et al., 2018). Furthermore, *Tm4sf2<sup>-/-</sup>* mice showed anhedonia- and depressive-like states. This is not very surprising, since one of the main hypothesis regarding ASD social avoidance is the inability of autistic people to experience pleasure from social relationship (Chevallier et al., 2012b). However, recently, this hypothesis has been extended also to non-social stimuli (Clements et al., 2018). Additionally, ASD patients have three to four times higher probability to experience depression (Hudson et al., 2019), suggesting that these pathologies might share common pathophysiological mechanisms.

Interestingly, the LHb is emerging as a strategic brain region that coordinates several areas involved in sociability, repetitive behaviors, anhedonia- and depressive-like states, such as ventral tegmental area (VTA), substantia nigra pars compacta (SNc) and raphe nuclei (Hu et al., 2020). Intriguingly, LHb is also involved in learning, memory and behavioral flexibility (Lecourtier et al., 2004; Baker et al., 2015; Mathis et al., 2015; Mathis and Lecourtier, 2017), suggesting an interplay with the hippocampus. Despite a LHb-hippocampal direct connection has not been described, several studies suggested that these regions could interact through theta waves neuronal coherence (Aizawa et al., 2013; Goutagny et al., 2013; Baker et al., 2019). Moreover, an altered LHb-hippocampal neuronal coherence could affect learning and memory in rodents (Goutagny et al., 2013). All these suggestions allowed us to hypothesize that an altered LHb function could be present in *Tm4sf2<sup>-/-</sup>* mice.

We analyzed LHb glutamatergic neurons given their higher predominance (Lecca et al., 2014) and their involvement in neuropsychiatric disorders (Meye et al., 2015; Lecca et al., 2016; Tchenio et al., 2017; Li et al., 2019; Valentinova et al., 2019). Firstly, we analyzed excitatory and inhibitory synaptic inputs in terms of mEPSCs/mIPSCs and GABA<sub>B</sub>-mediated GIRK potassium currents founding no changes between genotypes. This was extremely surprising for us, since we previously demonstrated reduced amplitude and frequency of mEPSCs in hippocampus (Murru et al., 2017), due to the role of TSPAN7 in PICK1-mediated trafficking of GluA2-containing AMPA receptors. However, glutamatergic input onto LHb mainly relies on

GluA2-lacking AMPARs (Li et al., 2011; Maroteaux and Mameli, 2012), thus supporting the unchanged mEPSCs amplitude and frequency in  $Tm4sf2^{-/-}$  mice.

Furthermore, we found a decreased number of Lhb tonic regular firing neurons accompanied by a concomitant increase of silent neurons in  $Tm4sf2^{-/-}$  mice. Noteworthy, even if not statistically significant, tonic irregular firing neurons almost doubled in  $Tm4sf2^{-/-}$  mice.

Interestingly, an altered Lhb firing pattern is correlated to psychiatric diseases, such as depression (Cui et al., 2018; Yang et al., 2018). We also found a decreased firing activity and an increased spiking accommodation in  $Tm4sf2^{-/-}$  mice Lhb neurons that correlated with learning defects (Tombaugh et al., 2005). In accordance, Lhb inactivation impairs hippocampal-dependent memory processes (Goutagny et al., 2013).

Afterwards, we found decreased AP amplitude, increased half width and slower kinetic.

Furthermore, we repeated the analysis on Lhb neuronal excitability at the light of the different firing pattern categories. Interestingly, while a clear downward trend in  $Tm4sf2^{-/-}$  mice Lhb AP firing frequency for all categories was present, the AP features were affected mainly in Lhb tonic (regular and irregular) firing neurons. These results might suggest an involvement of VGIC since even small modifications in their activity lead to dramatic alterations in AP shape and excitability (Goldman et al., 2001; Hill, 2001; Milesescu et al., 2010; Amendola et al., 2012; Lin et al., 2019). Coherently, we investigated VGNC and VGKC function, and we found decreased VGNC-mediated currents and slower gating kinetic in  $Tm4sf2^{-/-}$  mice, while VGKC activated at more hyperpolarized potentials and mediated more current. VGNC and VGKC impaired function well fits with the  $Tm4sf2^{-/-}$  mice Lhb neuronal phenotype. Worth of note, we identified the “A-type” current as the only  $K^+$  component affected in  $Tm4sf2^{-/-}$  mice Lhb neurons. This  $K^+$  component plays a key role in controlling neuronal activity (Coetzee et al., 1999; Hill, 2001; Kim et al., 2005; Drion et al., 2015; Rathour et al., 2016). Interestingly, A-type elimination strongly enhances the intrinsic neuronal excitability (Kim et al., 2005; Rathour et al., 2016). Then, it is plausible that an increase in A-type current might have an opposite effect. Despite VGNC and VGKC have distinct roles in AP kinetic, theoretically the total  $Na^+$  influx must be counteracted by a similar  $K^+$  outflow, giving rise to a physiological AP. When this equilibrium is disturbed, AP shape and neuronal firing might be strongly altered. Our results suggest that in  $Tm4sf2^{-/-}$  mice VGNC and VGKC gating alterations induce an increased overlap between the depolarizing  $Na^+$  and the repolarizing  $K^+$  currents, causing alterations in APs frequency and shape. On the other hand,  $Tm4sf2^{-/-}$  mice Lhb silent

neurons did not display AP kinetic alterations suggesting that VGIC might be unaffected in this neuronal category. For this reason, it is reasonable to believe that the VGIC functional alterations that we noticed might be restricted to Tm4sf2<sup>-/-</sup> mice LHb tonic neurons. However, the analysis of VGIC function, obtained pooling together data from all the neuronal firing categories, might eventually underestimate the phenomenon in Tm4sf2<sup>-/-</sup> mice LHb tonic neurons.

All together, these data demonstrates LHb dysfunction in Tm4sf2<sup>-/-</sup> mice, and it is likely that VGNC and VGKC could participate.

The main arising question is how TSPAN7 absence could induce these functional alterations in LHb. Tetraspanins, acting as molecular facilitators (Hemler, 2008), promote the proteins clusterization and favor their chance of interactions. Moreover, tetraspanins interact with ion channels modulating their function, such as TSPAN13 for instance (Mallmann et al., 2013). For that reason, we investigated if TSPAN7 absence could alter VGIC expression.

Interestingly, in agreement with the reduction in VGNC-mediated currents that we reported, we found a significant decrease of VGNC expression in the LHb of Tm4sf2<sup>-/-</sup> mice. On the contrary, no changes in the VGKC Kv4.2 subunit expression has been detected, even if we cannot exclude that other VGKC subunits might mediate the A-type current in the LHb.

Previously, we demonstrated that TSPAN7 directly interacts with PICK1 (Bassani et al., 2012). PICK1, in turn, regulates ion channels, such as the acid-sensing ion channels (ASICs) (Baron et al., 2002; Duggan et al., 2002; Hruska-Hageman et al., 2002; Hu et al., 2010), acting as a linker between PKC and ASICs. Moreover, PICK1 ablation alters ASICs function (Hu et al., 2010). Furthermore, PKC regulates VGNC and VGKC activity phosphorylating them (Numann et al., 1991; Levitan, 1994; Boland and Jackson, 1999; Schrader et al., 2009; Scheuer, 2011; Andersen et al., 2018). The increase in PKC function is reported to decrease the current peak and to slower the kinetic of VGNC (Numann et al., 1991), which mimics what we found in Tm4sf2<sup>-/-</sup> mice. Consistently, we found a PKC hyperactivity in Tm4sf2<sup>-/-</sup> mice. On the other hand, PKC is reported to decrease A-type K<sup>+</sup> current (Hoffman and Johnston, 1998; Deng et al., 2011). Interestingly, the Kv4.2 potassium channel subunit, that mediate the majority of A-type current in the hippocampus, and that we found expressed in the mouse habenula, presents three ERK/MAPK phosphorylation sites at amino acid residues T602, T607, and S616 (Adams et al., 2000; Schrader et al., 2006). Moreover, the phosphorylation of the S616 residue causes a shift of the activation voltage toward more hyperpolarized

potentials, similarly to what we noticed in Tm4sf2<sup>-/-</sup> mice (Schrader et al., 2006). Based on studies demonstrating the ability of PKCs to activate the extracellular signal-regulated kinase (ERK) (Yamaguchi et al., 1995; Schönwasser et al., 1998), we investigated ERK activity in Tm4sf2<sup>-/-</sup> mice and we found it increased. This result suggests that ERK might modulate VGKC activity in Tm4sf2<sup>-/-</sup> mice.

## 5. Conclusion

In conclusion, we demonstrated that Tm4sf2<sup>-/-</sup> mice show also ASD-like behavior, phenocopying the human pathology (Piton et al., 2011). Moreover, we found compromised LHB activity, highlighting significant alterations in VGNC and VGIC function and/or expression. Interestingly, we also noticed a PKC-ERK hyperactivity, which are well known regulators of VGIC. For that reasons, the functional alterations of Tm4sf2<sup>-/-</sup> mice LHB might be the result of an altered VGNC expression and/or an aberrant phosphorylation of VGIC. As mentioned above, the LHB acts as a relay, finely regulating and integrating neuronal signals coming from several brain regions (Hu et al., 2020), therefore, despite a direct connection between LHB function and ASD-like behaviors has to be proven, we can speculate that dysfunctions in this area could correlate with the impaired cognitive functions showed by Tm4sf2<sup>-/-</sup> mice. Considering the social impact of neurodevelopmental disorders, future studies will be necessary to unravel the specific LHB involvement in these pathologies.

## Acknowledgments:

We thank M. Mameli, P. Botta and E. Moretto for feedback on the manuscript and fruitful discussions.

## CRedit author statement:

Murru Luca: Conceptualization; Data curation; Formal analysis; Validation; Funding acquisition; Investigation; Methodology; Project administration; Writing original draft; Writing - review & editing.  
 Ponzoni Luisa: Data curation; Formal analysis; Investigation; Methodology; Editing.  
 Longatti Anna: Data curation; Formal analysis; Investigation; Methodology.  
 Mazzoleni Sara: Data curation; Formal analysis; Investigation; Methodology; Editing.  
 Giansante Giorgia: Data curation; Formal analysis; Investigation; Methodology; Editing.  
 Bassani Silvia: Data curation; Formal analysis; Editing.  
 Sala Marielvina: Data curation; Formal analysis; Editing.  
 Passafaro Maria: Conceptualization; Validation; Funding acquisition; Project administration; Resources; Writing - review & editing; Supervision.

## Funding:



This work was supported by Telethon Italy (Grant number GGP17283) to PM, Ministero della salute (Grant number GR-2016-02361366) to ML and Fondazione Zardi Gori (for providing fellowship to PL) and Regione Lombardia for providing fellowship to LA (Grant iPS Light ID 227333).

### **Declaration of Competing Interest:**

The authors declare no competing financial interests.

### **References**

- Adams JP, Anderson AE, Varga AW, Dineley KT, Cook RG, Pfaffinger PJ, Sweatt JD (2000) The A-type potassium channel Kv4.2 is a substrate for the mitogen-activated protein kinase ERK. *J Neurochem.*
- Aizawa H, Yanagihara S, Kobayashi M, Niisato K, Takahawa T, Harukuni R, McHugh TJ, Fukai T, Isomura Y, Okamoto H (2013) The synchronous activity of lateral habenular neurons is essential for regulating hippocampal theta oscillation. *J Neurosci.*
- Amendola J, Woodhouse A, Martin-Eauclaire MF, Goillard JM (2012) Ca<sup>2+</sup>/cAMP-sensitive covariation of I<sub>A</sub> and I<sub>H</sub> voltage dependences tunes rebound firing in dopaminergic neurons. *J Neurosci.*
- Amodeo DA, Jones JH, Sweeney JA, Fajozzino ME (2012) Differences in BTBR T+<sup>tf</sup>/J and C57BL/6J mice on probabilistic reversal learning and stereotyped behaviors. *Behav Brain Res.*
- Andersen MN, Skibsbjerg L, Salje A, Larsen MZ, Rasmussen HB, Jespersen T (2018) Regulation of Kv1.4 potassium channels by PKC and AMPK kinases. *Channels.*
- Aspromonte MC et al. (2019) Characterization of intellectual disability and autism comorbidity through gene panel sequencing. *Hum Mutat.*
- Baker PM, Mizumori SJY (2017) Control of behavioral flexibility by the lateral habenula. *Pharmacol Biochem Behav.*
- Baker PM, Oh SE, Kidder KS, Mizumori SJY (2015) Ongoing behavioral state information signaled in the lateral habenula guides choice flexibility in freely moving rats. *Front Behav Neurosci.*
- Baker PM, Rao Y, Rivera ZMG, Garcia EM, Mizumori SJY (2019) Selective Functional Interaction Between the Lateral Habenula and Hippocampus During Different Tests of Response Flexibility. *Front Mol Neurosci.*



- Baron A, Deval E, Salinas M, Lingueglia E, Voilley N, Lazdunski M (2002) Protein kinase C stimulates the acid-sensing ion channel ASIC2a via the PDZ domain-containing protein PICK1. *J Biol Chem*.
- Bassani S, Cingolani LA (2012) Tetraspanins: Interactions and interplay with integrins. *Int J Biochem Cell Biol*.
- Bassani S, Cingolani LA, Valnegri P, Folci A, Zapata J, Gianfelice A, Sala C, Goda Y, Passafaro M (2012) The X-Linked Intellectual Disability Protein TSPAN7 Regulates Excitatory Synapse Development and AMPAR Trafficking. *Neuron*.
- Bassani S, Zapata J, Gerosa L, Moretto E, Murru L, Passafaro M (2013) The neurobiology of x-linked intellectual disability. *Neuroscientist* 19.
- Benekareddy M, Stachniak TJ, Bruns A, Knoflach F, von Kienlin M, Künnecke B, Ghosh A (2018) Identification of a Corticohabenular Circuit Regulating Socially Directed Behavior. *Biol Psychiatry*.
- Berditchevski F (2001) Complexes of tetraspanins with integrins: More than meets the eye. *J Cell Sci*.
- Boland LM, Jackson KA (1999) Protein kinase C inhibits Kv1.1 potassium channel function. *Am J Physiol - Cell Physiol*.
- Bromberg-Martin ES, Matsumoto M, Nukuhara H, Hikosaka O (2010) Multiple Timescales of Memory in Lateral Habenula and Dopamine Neurons. *Neuron*.
- Charrin S, Jouannet S, Bouchoix C, Rubinstein E (2014) Tetraspanins at a glance. *J Cell Sci*.
- Chevallier C, Grèzes J, Molesworth C, Berthoz S, Happé F (2012a) Brief report: Selective social anhedonia in high functioning autism. *J Autism Dev Disord*.
- Chevallier C, Kohls G, Troiani V, Brodtkin ES, Schultz RT (2012b) The social motivation theory of autism. *Trends Cogn Sci*.
- Clements CC, Zoltowski AR, Yankowitz LD, Yerys BE, Schultz RT, Herrington JD (2018) Evaluation of the social motivation hypothesis of autism a systematic review and meta-analysis. In: *JAMA Psychiatry*.
- Coetzee WA, Amarillo Y, Chiu J, Chow A, Lau D, McCormack T, Moreno H, Nadal MS, Ozaita A, Pountney D, Saganich M, Vega-Saenz De Miera E, Rudy B (1999) Molecular diversity of K<sup>+</sup> channels. In: *Annals of the New York Academy of Sciences*.
- Cui Y, Yang Y, Ni Z, Dong Y, Cai G, Foncelle A, Ma S, Sang K, Tang S, Li Y, Shen Y, Berry H, Wu S, Hu H (2018) Astroglial Kir4.1 in the lateral habenula drives neuronal bursts in

depression. *Nature*.

- Deng P, Pang ZP, Lei Z, Shikano S, Xiong Q, Harvey BK, London B, Wang Y, Li M, Xu ZC (2011) Up-regulation of A-type potassium currents protects neurons against cerebral ischemia. *J Cereb Blood Flow Metab*.
- Drion G, O'Leary T, Marder E (2015) Ion channel degeneracy enables robust and tunable neuronal firing rates. *Proc Natl Acad Sci U S A*.
- Duggan A, García-Añoveros J, Corey DP (2002) The PDZ domain protein PICK1 and the sodium channel BNC1 interact and localize at mechanosensory terminals of dorsal root ganglion neurons and dendrites of central neurons. *J Biol Chem*.
- Goldman MS, Golowasch J, Marder E, Abbott LF (2001) Global structure, robustness, and modulation of neuronal models. *J Neurosci*.
- Goutagny R, Loureiro M, Jackson J, Chaumont J, Williams S, Isope P, Kelche C, Cassel JC, Lecourtier L (2013) Interactions between the lateral habenula and the Hippocampus: Implication for spatial memory processes. *Neuropsychopharmacology*.
- Hascoët M, Bourin M, Nic Dhonnchadha BA (2001) The mouse light-dark paradigm: A review. *Prog Neuro-Psychopharmacology Biol Psychiatry*.
- Hemler ME (2008) Targeting of tetraspanin proteins - Potential benefits and strategies. *Nat Rev Drug Discov*.
- Hill B (2001) *Ion Channels of excitable membranes*, third. Sinauer associates.
- Hoffman DA, Johnston D (1993) Downregulation of transient K<sup>+</sup> channels in dendrites of hippocampal CA1 pyramidal neurons by activation of PKA and PKC. *J Neurosci*.
- Hruska-Hageman AM, Wemmie JA, Price MP, Welsh MJ (2002) Interaction of the synaptic protein PICK1 (protein interacting with C kinase 1) with the non-voltage gated sodium channels BNC1 (brain Na<sup>+</sup> channel 1) and ASIC (acid-sensing ion channel). *Biochem J*.
- Hu H, Cui Y, Yang Y (2020) Circuits and functions of the lateral habenula in health and in disease. *Nat Rev Neurosci*.
- Hu ZL, Huang C, Fu H, Jin Y, Wu WN, Xiong QJ, Xie N, Long LH, Chen JG, Wang F (2010) Disruption of PICK1 attenuates the function of ASICs and PKC regulation of ASICs. *Am J Physiol - Cell Physiol*.
- Huang Z, Hoffman CA, Chelette BM, Thiebaud N, Fadool DA (2018) Elevated anxiety and impaired attention in super-smeller, Kv1.3 knockout mice. *Front Behav Neurosci*.
- Hudson CC, Hall L, Harkness KL (2019) Prevalence of Depressive Disorders in Individuals

- with Autism Spectrum Disorder: a Meta-Analysis. *J Abnorm Child Psychol*.
- Ji H, Shepard PD (2007) Lateral habenula stimulation inhibits rat midbrain dopamine neurons through a GABAA receptor-mediated mechanism. *J Neurosci*.
- Kawa R, Pisula E (2010) Locomotor activity, object exploration and space preference in children with autism and down syndrome. *Acta Neurobiol Exp (Wars)*.
- Kim J, Wei DS, Hoffman DA (2005) Kv4 potassium channel subunits control action potential repolarization and frequency-dependent broadening in rat hippocampal CA1 pyramidal neurones. *J Physiol*.
- Lecca S, Meye FJ, Mameli M (2014) The lateral habenula in addiction and depression: An anatomical, synaptic and behavioral overview. *Eur J Neurosci*.
- Lecca S, Pelosi A, Tchenio A, Moutkine I, Lujan R, Hervé D, Mameli M (2016) Rescue of GABAB and GIRK function in the lateral habenula by protein phosphatase 2A inhibition ameliorates depression-like phenotypes in mice. *Neu Med*.
- Lecourtier L, Neijt HC, Kelly PH (2004) Habenula lesions cause impaired cognitive performance in rats: Implications for schizophrenia. *Eur J Neurosci*.
- Lee SA, Suh Y, Lee S, Jeong J, Kim SJ, Kim SJ, Park SK (2017) Functional expression of dopamine D2 receptor is regulated by tetraspanin 7-mediated postendocytic trafficking. *FASEB J*.
- Levitan I (1994) Modulation of Ion Channels by Protein Phosphorylation and Dephosphorylation. *Annu Rev Physiol*.
- Li B, Piriz J, Mirrione M, Chung C, Proulx CD, Schulz D, Henn F, Malinow R (2011) Synaptic potentiation onto habenula neurons in the learned helplessness model of depression. *Nature*.
- Li J, Yang S, Liu X, Han Y, Li Y, Feng J, Zhao H (2019) Hypoactivity of the lateral habenula contributes to negative symptoms and cognitive dysfunction of schizophrenia in rats. *Exp Neurol*.
- Lin Z, Huang X, Zhou W, Zhang W, Liu Y, Bian T, Niu L, Meng L, Guo Y (2019) Ultrasound stimulation modulates voltage-gated potassium currents associated with action potential shape in hippocampal CA1 pyramidal neurons. *Front Pharmacol*.
- Liu GX, Cai GQ, Cai YQ, Sheng ZJ, Jiang J, Mei Z, Wang ZG, Guo L, Fei J (2007) Reduced anxiety and depression-like behaviors in mice lacking GABA transporter subtype 1. *Neuropsychopharmacology*.

- Mallmann RT, Wilmes T, Lichvarova L, Bühner A, Lohmüller B, Castonguay J, Lacinova L, Klugbauer N (2013) Tetraspanin-13 modulates voltage-gated CaV2.2 Ca<sup>2+</sup> channels. *Sci Rep*.
- Maroteaux M, Mameli M (2012) Cocaine evokes projection-specific synaptic plasticity of lateral habenula neurons. *J Neurosci*.
- Mathis V, Cosquer B, Avallone M, Cassel JC, Lecourtier L (2015) Excitatory transmission to the lateral habenula is critical for encoding and retrieval of spatial memory. *Neuropsychopharmacology*.
- Mathis V, Lecourtier L (2017) Role of the lateral habenula in memory through online processing of information. *Pharmacol Biochem Behav*.
- McFarlane HG, Kusek GK, Yang M, Phoenix JL, Bolivar VJ, Cawley JN (2008) Autism-like behavioral phenotypes in BTBR T+tf/J mice. *Genes Brain Behav*.
- Mefford HC, Batshaw ML, Hoffman EP (2012) Genomics, intellectual disability, and autism. *N Engl J Med*.
- Meye FJ, Valentinova K, Lecca S, Marion-Poll L, Maroteaux MJ, Musardo S, Moutkine I, Gardoni F, Huganir RL, Georges F, Mameli M (2015) Cocaine-evoked negative symptoms require AMPA receptor trafficking in the lateral habenula. *Nat Neurosci*.
- Milescu LS, Yamanishi T, Ptak K, Smith MC (2010) Kinetic properties and functional dynamics of sodium channels during repetitive spiking in a slow pacemaker neuron. *J Neurosci*.
- Mizumori SJY, Baker PM (2017) The Lateral Habenula and Adaptive Behaviors A Core Mechanism Underlying Flexible Response Systems. *Trends Neurosci*.
- Moretto E, Longatti A, Murru L, Chamma I, Sessa A, Zapata J, Hosy E, Sainlos M, Saint-Pol J, Rubinstein E, Chequet D, Broccoli V, Schiavo G, Thoumine O, Passafaro M (2019) TSPAN5 Enriched Microdomains Provide a Platform for Dendritic Spine Maturation through Neuroligin-1 Clustering. *Cell Rep*.
- Moretto E, Murru L, Martano G, Sassone J, Passafaro M (2018) Glutamatergic synapses in neurodevelopmental disorders. *Prog Neuro-Psychopharmacology Biol Psychiatry*.
- Murru L, Moretto E, Martano G, Passafaro M (2018) Tetraspanins shape the synapse. *Mol Cell Neurosci* 91.
- Murru L, Vezzoli E, Longatti A, Ponzoni L, Falqui A, Folci A, Moretto E, Bianchi V, Braidà D, Sala M, D'Adamo P, Bassani S, Francolini M, Passafaro M (2017) Pharmacological Modulation of AMPAR Rescues Intellectual Disability-Like Phenotype in Tm4sf2<sup>-/-</sup> Mice.

Cereb Cortex 27.

Namboodiri VMK, Rodriguez-Romaguera J, Stuber GD (2016) The habenula. *Curr Biol*.

Novacek DM, Gooding DC, Pflum MJ (2016) Hedonic capacity in the broader autism phenotype: Should social anhedonia be considered a characteristic feature? *Front Psychol*.

Numann R, Catterall WA, Scheuer T (1991) Functional modulation of brain sodium channels by protein kinase C phosphorylation. *Science* (80- ).

Oeseburg B, Dijkstra GJ, Groothoff JW, Reijneveld SA, Jansen DEMC (2011) Prevalence of chronic health conditions in children with intellectual disability: A systematic literature review. *Intellect Dev Disabil*.

Penzes P, Buonanno A, Passafaro M, Sala C, Sweet RA (2013) Developmental vulnerability of synapses and circuits associated with neuropsychiatric disorders. *J Neurochem*.

Pierce K, Courchesne E (2001) Evidence for a cerebellar role in reduced exploration and stereotyped behavior in autism. *Biol Psychiatry*.

Piton A et al. (2011) Systematic resequencing of X-chromosome synaptic genes in autism spectrum disorder and schizophrenia. *Mol Psychiatry*.

Pizzamiglio L, Focchi E, Murru L, Tamberini M, Passafaro M, Menna E, Matteoli M, Antonucci F (2016) New Role of ATM in Controlling GABAergic Tone during Development. *Cereb Cortex* 26.

Rathour RK, Malik R, Narayanan P (2016) Transient potassium channels augment degeneracy in hippocampal active dendritic spectral tuning. *Sci Rep*.

Scheuer T (2011) Regulation of sodium channel activity by phosphorylation. *Semin Cell Dev Biol*.

Schönwasser DC, Marais RM, Marshall CJ, Parker PJ (1998) Activation of the Mitogen-Activated Protein Kinase/Extracellular Signal-Regulated Kinase Pathway by Conventional, Novel, and Atypical Protein Kinase C Isotypes. *Mol Cell Biol*.

Schrader LA, Birnbaum SG, Nadin BM, Ren Y, Bui D, Anderson AE, Sweatt JD (2006) ERK/MAPK regulates the Kv4.2 potassium channel by direct phosphorylation of the pore-forming subunit. *Am J Physiol - Cell Physiol*.

Schrader LA, Ren Y, Cheng F, Bui D, Sweatt JD, Anderson AE (2009) Kv4.2 is a locus for PKC and ERK/MAPK cross-talk. *Biochem J* 417:705–715.

Schwartz CE, Neri G (2012) Autism and intellectual disability: Two sides of the same coin. *Am*

J Med Genet Part C Semin Med Genet.

- Shumake J, Ilango A, Scheich H, Wetzell W, Ohl FW (2010) Differential neuromodulation of acquisition and retrieval of avoidance learning by the lateral habenula and ventral tegmental area. *J Neurosci*.
- Silverman JL, Pride MC, Hayes JE, Puhger KR, Butler-Struben HM, Baker S, Crawley JN (2015) GABA B Receptor Agonist R-Baclofen Reverses Social Deficits and Reduces Repetitive Behavior in Two Mouse Models of Autism. *Neuropsychopharmacology*.
- Steru L, Chermat R, Thierry B, Simon P (1985) The tail suspension test: A new method for screening antidepressants in mice. *Psychopharmacology (Berl)*.
- Strekalova T, Gorenkova N, Schunk E, Dolgov O, Bartsch D (2003) Selective effects of citalopram in a mouse model of stress-induced anhedonia with a control for chronic stress. *Behav Pharmacol*.
- Tchenio A, Lecca S, Valentinova K, Mameli M (2017) Limiting habenular hyperactivity ameliorates maternal separation-driven depressive-like symptoms. *Nat Commun*.
- Termini CM, Gillette JM (2017) Tetraspanins function as regulators of cellular signaling. *Front Cell Dev Biol*.
- Tombaugh GC, Rowe WB, Rose GM (2005) The slow afterhyperpolarization in hippocampal CA1 neurons covaries with spatial learning ability in aged Fisher 344 rats. *J Neurosci*.
- Valentinova K, Tchenio A, Truscel M, Clerke JA, Lalive AL, Tzanoulinou S, Matera A, Moutkine I, Maroteaux L, Paolicelli PC, Volterra A, Bellone C, Mameli M (2019) Morphine withdrawal recruits lateral habenula cytokine signaling to reduce synaptic excitation and sociability. *Nat Neurosci*.
- Weiss T, Veh RW (2011) Morphological and electrophysiological characteristics of neurons within identified subnuclei of the lateral habenula in rat brain slices. *Neuroscience*.
- Yamaguchi K, Ogita K, Nakamura SI, Nishizuka Y (1995) The protein kinase C isoforms leading to map-kinase activation in CHO Cells. *Biochem Biophys Res Commun*.
- Yang Y, Cui Y, Sang K, Dong Y, Ni Z, Ma S, Hu H (2018) Ketamine blocks bursting in the lateral habenula to rapidly relieve depression. *Nature*.
- Zemni R et al. (2000) A new gene involved in X-linked mental retardation identified by analysis of an X;2 balanced translocation. *Nat Genet*.

Highlights

- Tm4sf2<sup>-/-</sup> mice display ASD-like behaviors.
- LHb neurons of Tm4sf2<sup>-/-</sup> mice present altered firing pattern and excitability.
- Voltage-gated ion channels function is impaired in Tm4sf2<sup>-/-</sup> mice.
- PKC-ERK signaling is hyperactive in Tm4sf2<sup>-/-</sup> mice.